

# Tip-Based Cleaning and Smoothing Improves Performance in Monolayer MoS<sub>2</sub> Devices

Sihan Chen, Jangyup Son, Siyuan Huang, Kenji Watanabe, Takashi Taniguchi, Rashid Bashir, Arend M. van der Zande, and William P. King\*

Cite This: *ACS Omega* 2021, 6, 4013–4021

Read Online

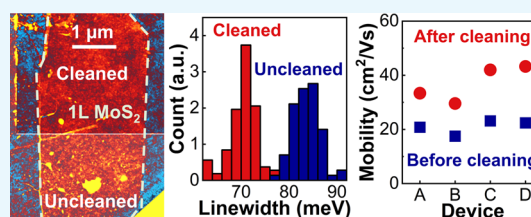
ACCESS |

Metrics & More

Article Recommendations

Supporting Information

**ABSTRACT:** Two-dimensional (2D) materials and heterostructures are promising candidates for nanoelectronics. However, the quality of material interfaces often limits the performance of electronic devices made from atomically thick 2D materials and heterostructures. Atomic force microscopy (AFM) tip-based cleaning is a reliable technique to remove interface contaminants and flatten heterostructures. Here, we demonstrate AFM tip-based cleaning applied to hBN-encapsulated monolayer MoS<sub>2</sub> transistors, which results in electrical performance improvements of the devices. To investigate the impact of cleaning on device performance, we compared the characteristics of as-transferred heterostructures and transistors before and after tip-based cleaning using photoluminescence (PL) and electronic measurements. The PL linewidth of monolayer MoS<sub>2</sub> decreased from 84 meV before cleaning to 71 meV after cleaning. The extrinsic mobility of monolayer MoS<sub>2</sub> field-effect transistors increased from 21 cm<sup>2</sup>/Vs before cleaning to 38 cm<sup>2</sup>/Vs after cleaning. Using the results from AFM topography, photoluminescence, and back-gated field-effect measurements, we infer that tip-based cleaning enhances the mobility of hBN-encapsulated monolayer MoS<sub>2</sub> by reducing interface disorder. Finally, we fabricate a MoS<sub>2</sub> field-effect transistor (FET) from a tip-cleaned heterostructure and achieved a device mobility of 73 cm<sup>2</sup>/Vs. The results of this work could be used to improve the electrical performance of heterostructure devices and other types of mechanically assembled van der Waals heterostructures.



## INTRODUCTION

The quality of material interfaces is critical to the performance of electronic devices and is particularly important for electronic devices made from two-dimensional (2D) materials. Common interface disorders that degrade device performance include interface Coulomb impurities, charge traps,<sup>1–4</sup> and local fluctuations in strain<sup>5,6</sup> and dielectric screening.<sup>7</sup> Carrier scattering due to interface impurities is significant, as atomically thick 2D materials do not have any bulk to screen impurities.<sup>8</sup> Carriers may also scatter at defects that arise from folding or wrinkling of the 2D material.<sup>9,10</sup>

Layers of 2D materials can be stacked together via van der Waals forces to create a wide variety of heterostructures that have novel or improved properties.<sup>11</sup> Clean and smooth interfaces are essential for the performance of electronic devices made from heterostructures.<sup>12–14</sup> Mechanical assembly is the most common way to fabricate van der Waals heterostructures,<sup>11,15</sup> but it often traps contaminants at the interfaces, which limits the carrier mobility, device performance, reproducibility, and reliability. Contaminants are trapped at the interfaces as a result of the competition between the elastic energy of the deformed 2D crystal and the adhesion energy between the 2D crystal and its substrate.<sup>16–18</sup> These contaminants come from the ambient environment or are residual materials from the assembly process.<sup>12,19–21</sup> Some research studies have been published on the nature of these

contaminants,<sup>12,17,22</sup> which include organic residue at the interfaces of stacked 2D layers.<sup>12,21,23</sup> To minimize interface contamination, it is necessary to either prevent the contamination from forming during fabrication or to remove it after fabrication. Strategies to prevent interface contamination include transferring in inert-gas filled glovebox or in vacuum,<sup>24,25</sup> as well as minimizing exposure of 2D materials to polymers and solvents used in transfer, such as dry pick-up.<sup>19,26,27</sup> Dry pick-up technique uses one layer of the 2D material to pick up another layer by van der Waals forces, which has enabled the fabrication of electronic devices with record-high performance and novel properties.<sup>14,26,28–30</sup> However, there exists substantial variation in electrical performance among the devices fabricated by pick-up technique,<sup>19,31</sup> which suggests a need to further improve the quality of the interfaces after assembly.

A few cleaning techniques are available to improve the interfaces of van der Waals heterostructures after assembly. As 2D materials are impermeable to all gases and liquids,<sup>32–34</sup>

Received: December 5, 2020

Accepted: January 20, 2021

Published: February 1, 2021



chemical and plasma-based techniques for cleaning the surfaces of 2D materials are not applicable for cleaning the interfaces.<sup>35–37</sup> Instead, thermal annealing is often used to reduce interface bubbles and increase the bubble-free area.<sup>8,12,31,38</sup> At the annealing temperature (typically 200–500 °C), small bubbles become mobile and migrate or aggregate into large bubbles.<sup>38</sup> Annealing relies on the random motion of interface bubbles and cannot reliably remove trapped contaminants from specific interface regions. Decomposition of contaminants during annealing may also produce radicals that damage 2D materials.<sup>39</sup> Alternatively, mechanical cleaning techniques, such as atomic force microscopy (AFM) tip-based cleaning, remove interface contaminants in a controlled fashion without damaging 2D materials.<sup>21,31,40,41</sup> In tip-based cleaning, an AFM tip squeezes trapped contaminants out from the interface of the targeted cleaning area, leaving the interface of the scanned area clean and flat.<sup>40</sup> Tip-based cleaning improved the mobility of bilayer graphene on hBN by a factor of 60–250%.<sup>42</sup> hBN-encapsulated graphene and few-layer MoS<sub>2</sub> devices also showed improvement in their magneto transport properties after tip-based cleaning.<sup>31</sup> Monolayers of 2D semiconductors, such as MoS<sub>2</sub>, WSe<sub>2</sub> and BP, are promising channel materials for nano-electronics, whose intrinsic carrier mobilities are however typically limited by extrinsic carrier scattering sources.<sup>43–46</sup> hBN encapsulation improves device performance of 2D semiconductors by reducing extrinsic disorders due to surface roughness, charged impurities, and interface charge traps, as hBN has fewer Coulomb impurities than SiO<sub>2</sub> and high- $\kappa$  dielectric substrates and is atomically flat.<sup>38,46,47</sup> There has however been no published research that investigates potential improvements for hBN-encapsulated 2D semiconductors using tip-based cleaning and smoothing.

This article reports significant improvement of interface qualities and electrical performance of hBN-encapsulated monolayer MoS<sub>2</sub> by tip-based cleaning. The cleaning process reduced nanometer-scale height fluctuations by an order of magnitude and reduced the photoluminescence linewidth of hBN-encapsulated monolayer MoS<sub>2</sub> from  $84 \pm 3$  to  $71 \pm 3$  meV, both of which indicate a reduction of interface disorder. The mobility of four monolayer MoS<sub>2</sub> FETs fabricated on the as-transferred heterostructure increased from an average of  $21 \pm 2$  to  $38 \pm 6$  cm<sup>2</sup>/Vs after cleaning, demonstrating that tip-based cleaning is effective in reducing interface disorder and enhancing the mobility of hBN-encapsulated monolayer MoS<sub>2</sub>. Finally, we demonstrate the utility of this approach by fabricating and testing a MoS<sub>2</sub> field-effect transistor (FET) fabricated on a tip-cleaned heterostructure.

## RESULTS

Figure 1 shows the tip-based cleaning of 2D heterostructures. The heterostructure system consists of monolayer MoS<sub>2</sub> encapsulated between monolayer (1L) hBN on top and multilayer (ML) hBN underneath. Figure 1a illustrates the concept of tip-based cleaning. As-transferred 2D heterostructures have surface and interface contaminants and voids between the 2D layers. The interface contaminants and voids aggregate into isolated pockets with typical lateral sizes from a few nanometers up to micrometers.<sup>16,19</sup> In addition to the voids and contaminants shown in Figure 1, there are also voids and contaminants between monolayer MoS<sub>2</sub> and the multilayer hBN substrate. By scanning the surface of the stacked 2D layers with an AFM tip in contact mode, the tip squeezes

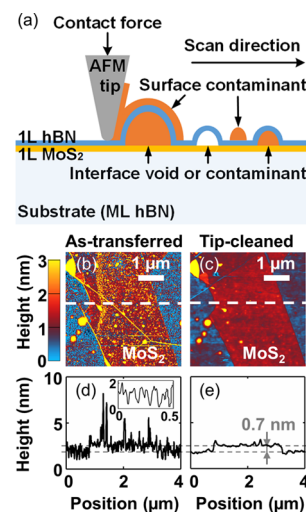


**Figure 1.** (a) Schematic of tip-based cleaning of 1L hBN covered 1L MoS<sub>2</sub> on a ML hBN substrate. AFM topography images of hBN-encapsulated monolayer MoS<sub>2</sub> (b) before and (c) after tip-based cleaning. (d, e) Line scans along the dashed lines in (b) and (c), respectively. Inset in (d) is the magnified view of the height profile over the position 0–0.5 μm.

trapped contaminants out from the interface of stacked 2D layers and flattens the stacked 2D layers while pushing surface contaminants along the scan direction. The AFM tip scans in a raster fashion, as in normal contact mode imaging. Surface and interface contaminants accumulate at the end of each scan line, leaving the scanned area clean and smooth.

We prepared the heterostructure stacks using an established dry pick-up technique summarized as follows.<sup>19,27</sup> First, we exfoliated hBN and MoS<sub>2</sub> flakes onto separate SiO<sub>2</sub> on Si substrates by Scotch tape. We used monolayers for the top hBN and 8–20 nm thick layers for the bottom hBN. Atomic force microscopy confirmed the monolayer nature of top hBN. Second, we picked up top hBN with a polycarbonate (PC) film coated on a polydimethylsiloxane (PDMS) lens.<sup>48</sup> Third, we sequentially picked up monolayer MoS<sub>2</sub> and bottom hBN by van der Waals forces between MoS<sub>2</sub> and hBN. Finally, we transferred monolayer MoS<sub>2</sub> encapsulated by top monolayer hBN and bottom multilayer hBN to the final 285 nm SiO<sub>2</sub> on the Si substrate. Figures S1, S2, and S3 show additional details of the fabrication. This heterostructure system has two benefits for studying the interfaces: First, this system has two interfaces between MoS<sub>2</sub> and hBN in the top 1–2 nm of the heterostructure, allowing the AFM to reveal details of interface inhomogeneity that are largely masked by much thicker top hBN.<sup>31</sup> Second, the top monolayer hBN serves as a tunnel layer to help inject charge carriers from contact metals into MoS<sub>2</sub>, allowing direct metal deposition to fabricate electronic devices, without additional processing steps.<sup>49,50</sup>

We performed the tip-based cleaning and measurement experiments using an Asylum MFP–3D AFM system. For all cleaning experiments, we used a cleaning force of 70–140 nN, and a scan speed of up to 28 μm/s. Mechanical cleaning depends strongly on the cleaning force but weakly on the speed. As long as the cleaning force is optimized, the scan speed should not significantly affect the cleaning. In general, AFM tip-based cleaning is limited by its throughput, so a faster scan is often better. The optimization of the cleaning force will be discussed later, while the scan speed was limited by the

control system of MFP-3D, which would be greatly increased using a video-rate AFM system.<sup>51</sup> The cleaning tips had a nominal tip radius of 8 nm. The density of scan lines was 5–7 nm/line, smaller than the tip radius to ensure that contaminants were pushed out of the cleaned region rather than accumulating between scan lines. After cleaning, we replaced the cleaning tip with an 8 nm radius tapping mode tip for imaging, which eliminated the potential for recontaminating the scanned area. Devices were imaged in tapping mode to minimize the interaction between the imaging tip and device surface. The imaging process did not affect the device surface, as repeated imaging of the same area produced identical AFM images.

Figure 1b–e shows example results of the heterostructure before and after tip-based cleaning with a 100 nN cleaning force. Figure 1b,c shows the topographic maps of the heterostructure before and after tip-based cleaning, respectively. Figure 1d,e shows the height profiles along the dashed lines in Figure 1b,c, respectively. Figure 1b,d exhibits height fluctuations in the bubble-free area of the as-transferred heterostructure. As shown in the inset of Figure 1d, the imaged height fluctuations have a lateral dimension of 50–100 nm and an amplitude of  $\sim 1$  nm. Figure 1c,e exhibits a much cleaner and smoother topography of the AFM-cleaned heterostructure, indicating that tip-based cleaning significantly reduces surface and interface contaminants and flattens the interfaces. The line scan in Figure 1e exhibits an average step height of 0.7 nm between monolayer MoS<sub>2</sub> and bottom hBN, indicating intimate contact between MoS<sub>2</sub> and hBN where interface impurities were absent.

We next examine the impact of the tip-based cleaning on the optical and electronic properties of the monolayer MoS<sub>2</sub> by comparing the photoluminescence and field effect transistor transport with and without tip-based cleaning.

First, Figure 2 compares the topography and photoluminescence between cleaned and uncleaned regions of a single heterostructure. For this measurement, we fabricated a heterostructure consisting of monolayer MoS<sub>2</sub> encapsulated by

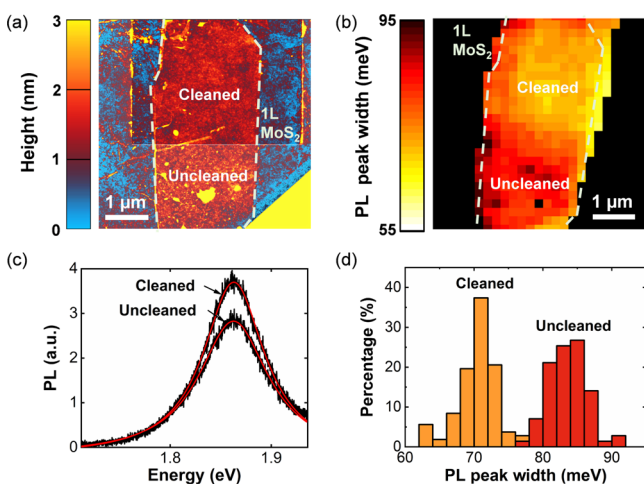


**Figure 2.** (a) AFM image of monolayer MoS<sub>2</sub> encapsulated by top monolayer hBN and 8 nm thick bottom hBN. The upper half of the heterostructure was processed by tip-based cleaning, while the lower half was uncleaned. (b) PL peak width map and (c) characteristic PL spectra with a single-peak Lorentzian fit (red curves) of hBN-encapsulated monolayer MoS<sub>2</sub> shown in (a). (d) Histogram of PL peak width of monolayer MoS<sub>2</sub> in the cleaned and uncleaned regions.

top monolayer hBN and 8 nm bottom hBN and performed tip-based cleaning on half of the device to create two regions, cleaned and uncleaned. This geometry facilitates side-by-side comparison under the same measurement conditions. We then measured the photoluminescence (PL) on both regions simultaneously.

Figure 2a shows the AFM topography of the heterostructure. The uncleaned region had a root-mean-square roughness  $R_{\text{rms}}$  of 2.03 nm, while the cleaned region had a much smaller roughness of 0.41 nm. Figure 2b–d shows the PL peak width (full-width-at-half-maximum) map, characteristic PL spectra, and histogram of PL peak width of monolayer MoS<sub>2</sub> in the cleaned and uncleaned regions. Each PL spectrum was fitted with a Lorentzian peak (red curves in Figure 2c). Both cleaned and uncleaned regions showed a single PL peak at  $1.863 \pm 0.004$  eV, corresponding to the A exciton peak in monolayer MoS<sub>2</sub>.<sup>52,53</sup> The cleaned region had an average PL peak width of  $70.5 \pm 2.9$  meV, while the uncleaned region had a peak width of  $83.7 \pm 2.8$  meV.

The photoluminescence of 2D materials is sensitive to strain, average doping, and disorder.<sup>54–57</sup> The peak width is correlated with the disorder within the material,<sup>54,55</sup> while the peak position is sensitive to doping and strain.<sup>56,57</sup> As a result, the photoluminescence maps reveal the impacts of tip-based cleaning on the electronic properties. First, the cleaned region had a much smaller PL peak width than the uncleaned region, indicating that tip-based cleaning reduces disorder in hBN-encapsulated monolayer MoS<sub>2</sub>.<sup>55,58</sup> Second, no A trion peak was detected in either cleaned or uncleaned region, indicating low electron doping in MoS<sub>2</sub> before cleaning and that tip-based cleaning did not induce electron doping in MoS<sub>2</sub>.<sup>59</sup> Third, there was no measurable difference in peak positions between the cleaned and uncleaned regions, indicating that tip-based cleaning did not significantly change average doping or strain. With a measurement precision of 4 meV, the induced strain and doping should be less than 0.08% and  $10^{12}$  cm<sup>-2</sup>, respectively.<sup>59–61</sup> Overall, the tip-based cleaning reduces interface disorder and does not induce average doping or strain.

Next, in Figures 3 and 4, we explore the optimal tip-based cleaning force for the heterostructure, as determined by

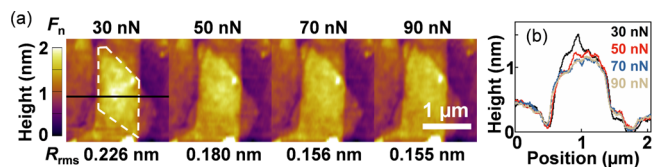


**Figure 3.** Critical cleaning force. (a) AFM images recorded by the cleaning tip with increasing contact force  $F_n$  from 30 to 90 nN. Surface roughness  $R_{\text{rms}}$  of the region enclosed by the dashed lines in are listed below each AFM image. (b) Line scans along the solid line in (a) with increasing contact force.

topography and photoluminescence. In Figure 3, we monitor changes in topography while scanning the same area of the heterostructure with increasing contact force  $F_n$  from 30 to 90 nN. Figure 3a shows the AFM images recorded by the cleaning tip as it scanned at each contact force. The surface roughness  $R_{\text{rms}}$  values of the heterostructure enclosed by the dashed lines in Figure 3a are listed below each AFM image. Figure 3b shows corresponding topographical changes along the solid line in Figure 3a. The surface roughness  $R_{\text{rms}}$  decreased significantly

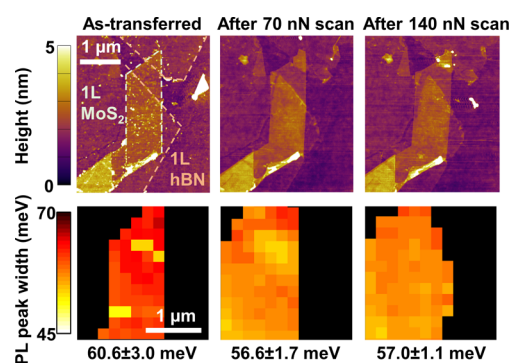


**Figure 4.** Determining the optimal cleaning force of the heterostructure by photoluminescence. AFM images and corresponding PL peak width maps of the same heterostructure as-transferred, after tip-based cleaning at 70 nN, and after additional cleaning at 140 nN. Average PL peak widths are listed below each PL map. Variations of outlines in PL maps resulted from misalignment and/or stage shift during measurement.

when  $F_n$  was increased from 30 to 50 nN and from 50 to 70 nN but decreased only slightly from 70 to 90 nN. The height profiles in Figure 3b also show no further topographical changes as  $F_n$  was increased from 70 to 90 nN.

Figure 4 shows the AFM topographies and corresponding PL peak width mappings of the same heterostructure as-transferred, after tip-based cleaning at 70 nN, and after additional cleaning at 140 nN. On average, the PL peak width of monolayer MoS<sub>2</sub> was  $60.6 \pm 3.0$  meV as-transferred,  $56.6 \pm 1.7$  meV after cleaning at 70 nN, and  $57.0 \pm 1.1$  meV after cleaning at 140 nN. Since additional cleaning at 140 nN did not further reduce the PL peak width, 70 nN was sufficient to optimize the PL of the heterostructure. In summary, the critical cleaning force for the heterostructure beyond which no improvement in topography or PL could be detected was around 70 nN.

While 70 nN is shown in this work to be the critical cleaning force for monolayer MoS<sub>2</sub> covered by monolayer hBN, the force needed to flatten heterostructures with multilayer top

hBN remains debatable. One article reports that the required cleaning force increases with the thickness of top hBN, and a  $2.1 \mu\text{N}$  force was used to flatten heterostructures with 18 nm thick top hBN.<sup>40</sup> Another work used a 50–150 nN force to flatten heterostructures with up to 50 nm thick top hBN.<sup>31</sup> The conflicting results may be explained by their differences in heterostructure fabrication: the former work used a water/solvent mixture in fabrication, which resulted in a few-nanometer-thick liquid contamination layer at the interfaces, while the latter used dry pick-up technique with minimal interface contamination. Future research should explore whether the optimal cleaning force is independent of the thickness of top hBN when the heterostructure is fabricated using dry pick-up.

To quantify the effects of tip-based cleaning on the electrical performance of hBN-encapsulated monolayer MoS<sub>2</sub>, we fabricated four separate field-effect transistors on an as-transferred heterostructure and compared their performance as fabricated and after tip-based cleaning. Figure 5 shows these devices. Figure 5a shows the schematic of the device structure and electrical measurement. The device consists of a monolayer MoS<sub>2</sub> channel, electrical contacts for the source and drain consisting of 30 nm gold on 5 nm nickel, a 13 nm hBN on 285 nm SiO<sub>2</sub> gate dielectric, and a degenerately p-doped silicon back gate. We take advantage of a recently reported technique, where the top monolayer hBN serves as a tunnel layer to help inject charge carriers from contact metals into MoS<sub>2</sub> and thus reduces contact resistance.<sup>49,50</sup> Figure 5b,c shows the AFM topographies of the FETs (Devices A–D) before and after tip-based cleaning, respectively. Surface roughness  $R_{\text{rms}}$  of the MoS<sub>2</sub> channel region decreased from 1.36 to 0.34 nm after cleaning, excluding trapped bubbles that persisted. Figure 5d shows the transfer curves of the FETs before (black) and after (red) tip-based cleaning.

We extracted four performance metrics of the FETs from the transfer curves: extrinsic field-effect mobility  $\mu = (L/W C_g V_{\text{ds}}) (dI_{\text{ds}}/dV_{\text{bg}})$ , threshold voltage  $V_{\text{th}}$ , subthreshold swing  $SS$ , and hysteresis  $H$ . We assumed a gate dielectric capacitance per unit area of 285 nm thick SiO<sub>2</sub> in series with 13 nm thick hBN ( $C_g$

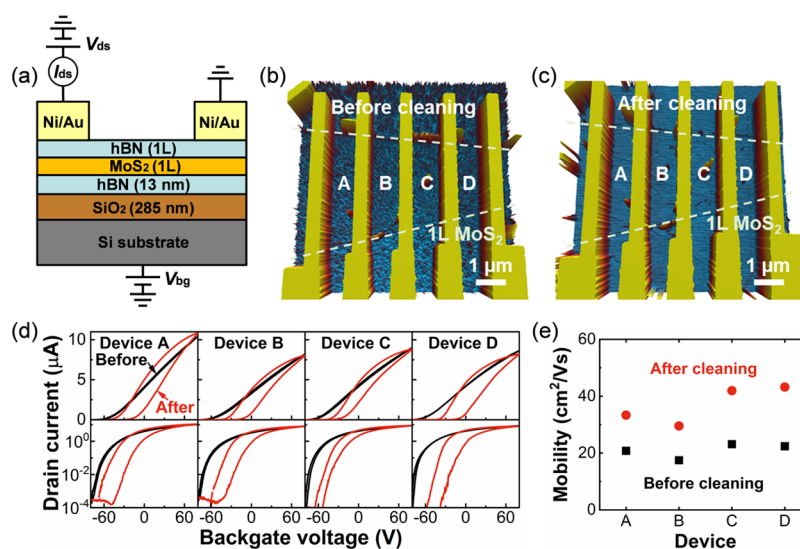


**Figure 5.** (a) Cross-sectional view of the FETs, along with the electrical connections to characterize the devices. AFM topography of the FETs (b) before and (c) after tip-based cleaning. (d) Transfer curves of the FETs before (black) and after (red) tip-based cleaning in both linear and semi-log scale.  $V_{\text{ds}} = 0.1$  V. (e) Extrinsic mobilities of the FETs before and after tip-based cleaning.

= 11.6 nF/cm<sup>2</sup>).<sup>62</sup> The tip-based cleaning affects mobility, threshold voltage, subthreshold swing, and hysteresis of the FETs measured in air. As shown in Figure 5e, the extrinsic mobility of every FET consistently increased after tip-based cleaning, by 60–93%. To exclude the effect of contact resistance, we further extracted the intrinsic mobilities using the Y-function method,<sup>75</sup> as shown in Figure S7. On average, before tip-based cleaning, the four FETs had an extrinsic mobility of  $21 \pm 2$  cm<sup>2</sup>/Vs, an intrinsic mobility of  $24 \pm 3$  cm<sup>2</sup>/Vs, a threshold voltage of  $-54.2 \pm 4.5$  V in forward sweep and  $-52.6 \pm 4.8$  V in reverse sweep, a subthreshold swing of  $3.6 \pm 1.3$  V/dec, and a hysteresis of  $1.6 \pm 0.9$  V. After tip-based cleaning, the FETs had an extrinsic mobility of  $38 \pm 6$  cm<sup>2</sup>/Vs, an intrinsic mobility of  $46 \pm 5$  cm<sup>2</sup>/Vs, a threshold voltage of  $-35.7 \pm 1.0$  V in forward sweep and  $-10.7 \pm 5.5$  V in reverse sweep, a subthreshold swing of  $7.0 \pm 1.5$  V/dec, and a hysteresis of  $25.1 \pm 5.3$  V.

We ascribe the improvement in mobility to reduced interface disorder by tip-based cleaning. Cleaning and flattening of the interfaces reduced local strain fluctuations, spatial inhomogeneities in dielectric screening, and interface Coulomb impurities.<sup>4,6,7</sup> As shown in a recent study,<sup>63</sup> the removal of surface contaminants does not improve the electron mobility of MoS<sub>2</sub> likely because ambient adsorbates could easily readsorb onto the surfaces after tip-based cleaning and still scatter charge carriers.<sup>64–66</sup> Unexpectedly, threshold voltage, subthreshold swing, and hysteresis are all increased after tip-based cleaning. The threshold voltage increased by an average of 18.4 V in forward sweep and 41.9 V in reverse sweep, the subthreshold swing nearly doubled, and the hysteresis increased by an average of 23.5 V. Previous reports show that annealing of MoS<sub>2</sub> or graphene on hBN reduces p-type doping, inducing a negative shift in threshold voltage.<sup>8,13,38</sup> It is peculiar that the initial hysteresis before cleaning is small since these devices had only a monolayer of hBN on top, compared with the much thicker layers of hBN >10 nm typically used in encapsulation.<sup>38,67</sup> We hypothesize that the positive shift in threshold voltage and the increase in subthreshold swing and hysteresis are all resulted from increased ambient effects after tip-based cleaning. The initial surface adsorbates that were cleaned away degraded the mobility but were relatively immobile. After tip-based cleaning, the effects of ambient adsorbates increased. Ambient adsorbates served as p-type dopants and charge traps,<sup>64–66</sup> leading to positive shift in threshold voltage and increased subthreshold swing and hysteresis after tip-based cleaning. In general, the increased role of ambient adsorbates is a tradeoff of using the monolayer top hBN, which had the advantage of reduced contact resistance<sup>49,50</sup> and enabled easy visualization of the interfaces. For applications, tip-based cleaning should be combined with thicker top hBN encapsulation.

For the device in Figure 5, we deposited the electrodes before cleaning to enable before and after comparison of device behavior. However, any residue or interfacial disorder under the electrodes will still affect contact resistance and thus limit device performance.<sup>68</sup> To examine the role of precleaning the interface, we fabricated a FET in the tip-cleaned region of the heterostructure shown in Figure 2. Figure 6 shows the transfer curve of the FET characterized in air in a two-probe configuration in which a drain-source bias was applied across the outer two leads, leaving the inner two leads floating. The inset shows the SEM image of the FET, exhibiting a channel width  $W$  of 2.42  $\mu\text{m}$  and a channel length  $L$  of 0.99  $\mu\text{m}$ . The

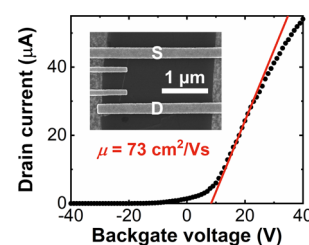


**Figure 6.** Transfer curve of a FET fabricated in the tip-cleaned region of the heterostructure shown in Figure 2.  $V_{\text{ds}} = 1$  V. Inset: SEM image of the FET.

device achieved an extrinsic electron mobility of 73 cm<sup>2</sup>/Vs, which is among the highest reported room-temperature extrinsic two-probe mobility values for monolayer MoS<sub>2</sub> (see Table S1).<sup>14,26,38,50,69–74</sup> We extracted the intrinsic mobility without the effect of contact resistance using the Y-function method<sup>75</sup> (see Figure S6) and obtained a high intrinsic electron mobility of 102 cm<sup>2</sup>/Vs. If we account for the differences in device geometry and  $V_{\text{ds}}$  (0.1 V in Figure 5 and 1 V in Figure 6), the transfer curve in Figure 6 is not very different from the ones after tip-based cleaning in Figure 5. The device in Figure 6 showed higher mobility than the devices in Figure 5, which likely resulted from lower contact resistance. However, we cannot rule out the possibility of device-to-device variations, which is ubiquitous in both exfoliated and synthetic monolayer MoS<sub>2</sub>.<sup>71,72,76</sup> Since top monolayer hBN is not sufficiently thick to screen charged impurities from ambient air,<sup>77</sup> which significantly limit the electrical performance of monolayer MoS<sub>2</sub>,<sup>64,65</sup> we expect further improvement in electron mobility after passivation with thick hBN or high- $k$  dielectrics.<sup>4,69,74,78</sup>

## DISCUSSION

The major advantage for AFM tip-based cleaning and smoothing of the van der Waals heterostructure is that it can be applied to a wide variety of van der Waals heterostructures assembled by various techniques. Tip-based learning is purely mechanical and insensitive to the chemistry of the contaminants and 2D layers. The cleaning procedure could be used not only for lateral FETs like hBN-encapsulated MoS<sub>2</sub> but also for vertical heterojunction transistors,<sup>79–81</sup> which are increasingly important for high-frequency applications. Other types of van der Waals heterostructures can also benefit from reduced interface impurities by tip-based cleaning.<sup>11,41,82</sup> AFM tip-based cleaning also has some limitations. First, it is challenging to remove bubbles much larger than the AFM tip radius. Thus, this cleaning technique is more suitable with van der Waals heterostructures without micron-scale interface impurities. Other techniques such as thermal annealing<sup>31,38</sup> and microdome cleaning<sup>83</sup> can be used to remove microbubbles trapped in between van der Waals heterostructures. Second, if the top 2D layer is fragile, the cleaning tip could damage the 2D material before interface contaminants are removed. Third, this technique is limited by low throughput ( $\sim 6 \mu\text{m}^2/\text{min}$  in this work), which is typical of all scanning probe-based techniques.<sup>84</sup>

## CONCLUSIONS

We demonstrated reliable cleaning and smoothing of the interfaces of hBN-encapsulated monolayer MoS<sub>2</sub>, by scanning the heterostructure with an AFM tip in contact mode. The

AFM tip-based cleaning reduced interface disorder as evidenced by reduced height fluctuations of the heterostructure and reduced photoluminescence linewidth of monolayer MoS<sub>2</sub>. The mobility of hBN-encapsulated monolayer MoS<sub>2</sub> improved substantially after tip-based cleaning. Combining the results from AFM topography, photoluminescence, and back-gated field-effect measurements, we infer that tip-based cleaning enhances the mobility of hBN-encapsulated monolayer MoS<sub>2</sub> by reducing interface disorder. Finally, we surmise that tip-based cleaning will also significantly improve the electrical properties of other mechanically assembled van der Waals heterostructures by cleaning and flattening their interfaces.

## METHODS

**Fabrication of the Heterostructures.** We assembled and transferred the heterostructures onto SiO<sub>2</sub> on Si substrates using established van der Waals pick-up techniques.<sup>19,27</sup> First, we exfoliated 2D flakes onto separate SiO<sub>2</sub> on Si substrates by Scotch tape. We used 90 nm thick oxide substrates with hBN exfoliation<sup>85</sup> and 285 nm thick oxide substrates with MoS<sub>2</sub> exfoliation for sufficient optical contrast to identify number of layers. We used monolayers for top hBN and 8–20 nm thick layers for bottom hBN. Atomic force microscopy confirmed the monolayer nature of top hBN (see Figure S3). Second, we prepared a PDMS lens on a glass slide and coated a layer of the PC film onto the PDMS lens.<sup>48</sup> Then, we fixed the glass slide with PC on PDMS stamp onto a micromanipulator. Third, we sequentially picked up 1L hBN, 1L MoS<sub>2</sub>, and ML hBN with the PC film on a PDMS lens at 90 °C. Fourth, we contacted 1L MoS<sub>2</sub> encapsulated by top 1L hBN and bottom ML hBN with the final 285 nm SiO<sub>2</sub> on the Si substrate at 90 °C and melted the PC film at 170 °C to complete transfer. Last, we removed the PC film on the heterostructure in a chloroform bath at room temperature for 24 h.

**Tip-Based Cleaning and Measurements.** All tip-based cleaning and measurement experiments were performed using an Asylum MFP–3D AFM system. For all cleaning experiments, we used a cleaning force of 70–140 nN and a scan speed of up to 28 μm/s. The cleaning tips (RFESP-7S, Bruker) had a nominal tip radius of 8 nm and a spring constant of 3 N/m. The density of scan lines was 5–7 nm/line, smaller than the tip radius to ensure that contaminants were pushed out of the cleaned region rather than accumulating between scan lines. After cleaning, we replaced the cleaning tip with an 8 nm radius tapping mode tip (HQ:NSC15/AL\_BS, MikroMasch) for imaging, which eliminated the potential for recontaminating the scanned area.

**Photoluminescence Measurements.** We performed PL measurements on a confocal Raman microscope (Nanophoton Raman 11) using a 532 nm laser with a 100× objective at an excitation power of 0.5 mW with a grating of 600 L/mm. The lateral resolution of the equipment was 350 nm. The PL map in Figure 2 had a pixel size of 0.2 μm and an acquisition time of 0.1 s per pixel. The PL maps in Figure 3 had a pixel size of 0.2 μm and an acquisition time of 3 s per pixel. Longer acquisition time increased signal but induced obvious stage drift. We performed all the measurements at room temperature in ambient laboratory conditions.

**Fabrication of MoS<sub>2</sub> Transistors and Electrical Measurement.** First, we patterned large contact pads and leads consisting of 30 nm Au on 5 nm Ni onto a 285 nm SiO<sub>2</sub> on the degenerately p-doped silicon substrate using optical

lithography. Second, we transferred the hBN-encapsulated monolayer MoS<sub>2</sub> onto prepatterned SiO<sub>2</sub> on the Si substrate. Third, we defined the contact electrodes to MoS<sub>2</sub> consisting of 30 nm Au on 5 nm Ni by e-beam lithography (eLINE, Raith) using a polymethyl methacrylate (PMMA) resist (A4 950k, Microchem) at an accelerating voltage of 20 kV, a beam current of 30 pA, and a dose of 240 μC/cm<sup>2</sup>. We performed all the electrical measurements in air at room temperature using a semiconductor parameter analyzer (Agilent, 4155C).

## ASSOCIATED CONTENT

### Supporting Information

The Supporting Information is available free of charge at <https://pubs.acs.org/doi/10.1021/acsomega.0c05934>.

Schematic of heterostructure preparation, optical images, additional AFM images, Raman spectroscopy, output curves, extractions of intrinsic mobility, additional surface roughness data, and Tables S1 and S2 (PDF)

## AUTHOR INFORMATION

### Corresponding Author

**William P. King** – Department of Mechanical Science and Engineering, University of Illinois at Urbana-Champaign, Urbana, Illinois 61801, United States; [orcid.org/0000-0001-8606-1290](https://orcid.org/0000-0001-8606-1290); Email: [wpk@illinois.edu](mailto:wpk@illinois.edu)

### Authors

**Sihan Chen** – Department of Mechanical Science and Engineering, University of Illinois at Urbana-Champaign, Urbana, Illinois 61801, United States

**Jangyup Son** – Department of Mechanical Science and Engineering, University of Illinois at Urbana-Champaign, Urbana, Illinois 61801, United States

**Siyuan Huang** – Department of Mechanical Science and Engineering, University of Illinois at Urbana-Champaign, Urbana, Illinois 61801, United States

**Kenji Watanabe** – National Institute for Materials Science, Tsukuba, Ibaraki 305-0044, Japan; [orcid.org/0000-0003-3701-8119](https://orcid.org/0000-0003-3701-8119)

**Takashi Taniguchi** – National Institute for Materials Science, Tsukuba, Ibaraki 305-0044, Japan; [orcid.org/0000-0002-1467-3105](https://orcid.org/0000-0002-1467-3105)

**Rashid Bashir** – Department of Mechanical Science and Engineering and Department of Bioengineering, University of Illinois at Urbana-Champaign, Urbana, Illinois 61801, United States

**Arend M. van der Zande** – Department of Mechanical Science and Engineering, University of Illinois at Urbana-Champaign, Urbana, Illinois 61801, United States; [orcid.org/0000-0001-5104-9646](https://orcid.org/0000-0001-5104-9646)

Complete contact information is available at: <https://pubs.acs.org/doi/10.1021/acsomega.0c05934>

### Notes

The authors declare no competing financial interest.

## ACKNOWLEDGMENTS

This work was supported in part by Taiwan Semiconductor Manufacturing Company (TSMC) under grant no. 089401. J.S. acknowledges support from the Korea Institute of Science and Technology Institution Program (2K02420, 2Z06030).

This work was carried out in part in the Materials Research Laboratory Central Facilities at the University of Illinois.

## REFERENCES

- (1) Terman, L. M. An Investigation of Surface States at a Silicon/Silicon Oxide Interface Employing Metal-Oxide-Silicon Diodes. *Solid-State Electron.* **1962**, *5*, 285–299.
- (2) Nicollian, E. H.; Goetzberger, A. The Si-SiO<sub>2</sub> Interface - Electrical Properties as Determined by the Metal-Insulator-Silicon Conductance Technique. *Bell Syst. Tech. J.* **1967**, *46*, 1055–1133.
- (3) Veturly, R.; Zhang, N. Q.; Keller, S.; Mishra, U. K. The Impact of Surface States on the DC and RF Characteristics of AlGaIn/GaN HFETs. *IEEE Trans. Electron Devices* **2001**, *48*, S60–S66.
- (4) Yu, Z.; Ong, Z.-Y.; Li, S.; Xu, J.-B.; Zhang, G.; Zhang, Y.-W.; Shi, Y.; Wang, X. Analyzing the Carrier Mobility in Transition-Metal Dichalcogenide MoS<sub>2</sub> Field-Effect Transistors. *Adv. Funct. Mater.* **2017**, *27*, 1604093.
- (5) Couto, N. J. G.; Costanzo, D.; Engels, S.; Ki, D. K.; Watanabe, K.; Taniguchi, T.; Stampfer, C.; Guinea, F.; Morpurgo, A. F. Random Strain Fluctuations as Dominant Disorder Source for High-Quality on-Substrate Graphene Devices. *Phys. Rev. X* **2014**, *4*, No. 041019.
- (6) Wang, L.; Makk, P.; Zihlmann, S.; Baumgartner, A.; Indolese, D. I.; Watanabe, K.; Taniguchi, T.; Schönenberger, C. Mobility Enhancement in Graphene by in Situ Reduction of Random Strain Fluctuations. *Phys. Rev. Lett.* **2020**, *124*, 157701.
- (7) Raja, A.; Waldecker, L.; Zipfel, J.; Cho, Y.; Brem, S.; Ziegler, J. D.; Kulig, M.; Taniguchi, T.; Watanabe, K.; Malic, E.; et al. Dielectric Disorder in Two-Dimensional Materials. *Nat. Nanotechnol.* **2019**, *14*, 832–837.
- (8) Dean, C. R.; Young, A. F.; Meric, I.; Lee, C.; Wang, L.; Sorgenfrei, S.; Watanabe, K.; Taniguchi, T.; Kim, P.; Shepard, K. L.; et al. Boron Nitride Substrates for High-Quality Graphene Electronics. *Nat. Nanotechnol.* **2010**, *5*, 722–726.
- (9) Katsnelson, M. I.; Geim, A. K. Electron Scattering on Microscopic Corrugations in Graphene. *Philos. Trans. R. Soc. A Math. Phys. Eng. Sci.* **2008**, *366*, 195–204.
- (10) Zhu, W.; Low, T.; Perebeinos, V.; Bol, A. A.; Zhu, Y.; Yan, H.; Tersoff, J.; Avouris, P. Structure and Electronic Transport in Graphene Wrinkles. *Nano Lett.* **2012**, *12*, 3431–3436.
- (11) Novoselov, K. S.; Mishchenko, A.; Carvalho, A.; Castro Neto, A. H. 2D Materials and van Der Waals Heterostructures. *Science* **2016**, *353*, aac9439.
- (12) Haigh, S. J.; Gholinia, A.; Jalil, R.; Romani, S.; Britnell, L.; Elias, D. C.; Novoselov, K. S.; Ponomarenko, L. A.; Geim, A. K.; Gorbachev, R. Cross-Sectional Imaging of Individual Layers and Buried Interfaces of Graphene-Based Heterostructures and Superlattices. *Nat. Mater.* **2012**, *11*, 764–767.
- (13) Wang, L.; Meric, I.; Huang, P. Y.; Gao, Q.; Gao, Y.; Tran, H.; Taniguchi, T.; Watanabe, K.; Campos, L. M.; Muller, D. A.; et al. One-Dimensional Electrical Contact to a Two-Dimensional Material. *Science* **2013**, *342*, 614–617.
- (14) Cui, X.; Lee, G.-H.; Kim, Y. D.; Arefe, G.; Huang, P. Y.; Lee, C.-H.; Chenet, D. A.; Zhang, X.; Wang, L.; Ye, F.; et al. Multi-Terminal Transport Measurements of MoS<sub>2</sub> Using a van Der Waals Heterostructure Device Platform. *Nat. Nanotechnol.* **2015**, *10*, 534–540.
- (15) Weston, A.; Zou, Y.; Enaldiev, V.; Summerfield, A.; Clark, N.; Zólyomi, V.; Graham, A.; Yelgel, C.; Magorrian, S.; Zhou, M.; et al. Atomic Reconstruction in Twisted Bilayers of Transition Metal Dichalcogenides. *Nat. Nanotechnol.* **2020**, *15*, 592–597.
- (16) Khestanova, E.; Guinea, F.; Fumagalli, L.; Geim, A. K.; Grigorieva, I. V. Universal Shape and Pressure inside Bubbles Appearing in van Der Waals Heterostructures. *Nat. Commun.* **2016**, *7*, 12587–12510.
- (17) Sanchez, D. A.; Dai, Z.; Wang, P.; Cantu-Chavez, A.; Brennan, C. J.; Huang, R.; Lu, N. Mechanics of Spontaneously Formed Nanoblisters Trapped by Transferred 2D Crystals. *Proc. Natl. Acad. Sci. U. S. A.* **2018**, *115*, 7884–7889.
- (18) Kretinin, A. V.; Cao, Y.; Tu, J. S.; Yu, G. L.; Jalil, R.; Novoselov, K. S.; Haigh, S. J.; Gholinia, A.; Mishchenko, A.; Lozada, M.; et al. Electronic Properties of Graphene Encapsulated with Different Two-Dimensional Atomic Crystals. *Nano Lett.* **2014**, *14*, 3270–3276.
- (19) Pizzocchero, F.; Gammelgaard, L.; Jessen, B. S.; Caridad, J. M.; Wang, L.; Hone, J.; Bøggild, P.; Booth, T. J. The Hot Pick-up Technique for Batch Assembly of van Der Waals Heterostructures. *Nat. Commun.* **2016**, *7*, 11894.
- (20) Ghorbanfekr-Kalashami, H.; Vasu, K. S.; Nair, R. R.; Peeters, F. M.; Neek-Amal, M. Dependence of the Shape of Graphene Nanobubbles on Trapped Substance. *Nat. Commun.* **2017**, *8*, 15844–15811.
- (21) Schwartz, J. J.; Chuang, H. J.; Rosenberger, M. R.; Sivaram, S. V.; McCreary, K. M.; Jonker, B. T.; Centrone, A. Chemical Identification of Interlayer Contaminants within van Der Waals Heterostructures. *ACS Appl. Mater. Interfaces* **2019**, *11*, 25578–25585.
- (22) Cao, P.; Xu, K.; Varghese, J. O.; Heath, J. R. The Microscopic Structure of Adsorbed Water on Hydrophobic Surfaces under Ambient Conditions. *Nano Lett.* **2011**, *11*, 5581–5586.
- (23) Gasparutti, I.; Song, S. H.; Neumann, M.; Wei, X.; Watanabe, K.; Taniguchi, T.; Lee, Y. H. How Clean Is Clean? Recipes for van Der Waals Heterostructure Cleanliness Assessment. *ACS Appl. Mater. Interfaces* **2020**, *12*, 7701–7709.
- (24) Jung, Y.; Choi, M. S.; Nipane, A.; Borah, A.; Kim, B.; Zangiabadi, A.; Taniguchi, T.; Watanabe, K.; Yoo, W. J.; Hone, J.; et al. Transferred via Contacts as a Platform for Ideal Two-Dimensional Transistors. *Nat. Electron.* **2019**, *2*, 187–194.
- (25) Kang, K.; Lee, K. H.; Han, Y.; Gao, H.; Xie, S.; Muller, D. A.; Park, J. Layer-by-Layer Assembly of Two-Dimensional Materials into Wafer-Scale Heterostructures. *Nature* **2017**, *550*, 229–233.
- (26) Jain, A.; Szabó, A.; Parzefall, M.; Bonvin, E.; Taniguchi, T.; Watanabe, K.; Bharadwaj, P.; Luisier, M.; Novotny, L. One-Dimensional Edge Contacts to a Monolayer Semiconductor. *Nano Lett.* **2019**, *19*, 6914–6923.
- (27) Kim, K.; Yankowitz, M.; Fallahzad, B.; Kang, S.; Movva, H. C. P.; Huang, S.; Larentis, S.; Corbet, C. M.; Taniguchi, T.; Watanabe, K.; et al. Van Der Waals Heterostructures with High Accuracy Rotational Alignment. *Nano Lett.* **2016**, *16*, 1989–1995.
- (28) Cao, Y.; Fatemi, V.; Fang, S.; Watanabe, K.; Taniguchi, T.; Kaxiras, E.; Jarillo-Herrero, P. Unconventional Superconductivity in Magic-Angle Graphene Superlattices. *Nature* **2018**, *556*, 43–50.
- (29) Crossno, J.; Shi, J. K.; Wang, K.; Liu, X.; Harzheim, A.; Lucas, A.; Sachdev, S.; Kim, P.; Taniguchi, T.; Watanabe, K.; et al. Observation of the Dirac Fluid and the Breakdown of the Wiedemann-Franz Law in Graphene. *Science* **2016**, *351*, 1058–1061.
- (30) Cao, Y.; Fatemi, V.; Demir, A.; Fang, S.; Tomarken, S. L.; Luo, J. Y.; Sanchez-Yamagishi, J. D.; Watanabe, K.; Taniguchi, T.; Kaxiras, E.; et al. Correlated Insulator Behaviour at Half-Filling in Magic-Angle Graphene Superlattices. *Nature* **2018**, *556*, 80–84.
- (31) Kim, Y.; Herlinger, P.; Taniguchi, T.; Watanabe, K.; Smet, J. H. Reliable Postprocessing Improvement of van Der Waals Heterostructures. *ACS Nano* **2019**, *13*, 14182–14190.
- (32) Bunch, J. S.; Verbridge, S. S.; Alden, J. S.; Van Der Zande, A. M.; Parpia, J. M.; Craighead, H. G.; McEuen, P. L. Impermeable Atomic Membranes from Graphene Sheets. *Nano Lett.* **2008**, *8*, 2458–2462.
- (33) Zhao, Y.; Xie, Y.; Liu, Z.; Wang, X.; Chai, Y.; Yan, F. Two-Dimensional Material Membranes: An Emerging Platform for Controllable Mass Transport Applications. *Small* **2014**, *10*, 4521–4542.
- (34) Lloyd, D.; Liu, X.; Christopher, J. W.; Cantley, L.; Wadehra, A.; Kim, B. L.; Goldberg, B. B.; Swan, A. K.; Bunch, J. S. Band Gap Engineering with Ultralarge Biaxial Strains in Suspended Monolayer MoS<sub>2</sub>. *Nano Lett.* **2016**, *16*, 5836–5841.
- (35) Chen, P. C.; Lin, C. P.; Hong, C. J.; Yang, C. H.; Lin, Y. Y.; Li, M. Y.; Li, L. J.; Yu, T. Y.; Su, C. J.; Li, K. S.; et al. Effective N-Methyl-2-Pyrrolidone Wet Cleaning for Fabricating High-Performance Monolayer MoS<sub>2</sub> Transistors. *Nano Res.* **2019**, *12*, 303–308.

- (36) Xiao, Z.; Wan, Q.; Durkan, C. Cleaning Transferred Graphene for Optimization of Device Performance. *Adv. Mater. Interfaces* **2019**, *6*, 1801794.
- (37) Lim, Y. D.; Lee, D. Y.; Shen, T. Z.; Ra, C. H.; Choi, J. Y.; Yoo, W. J. Si-Compatible Cleaning Process for Graphene Using Low-Density Inductively Coupled Plasma. *ACS Nano* **2012**, *6*, 4410–4417.
- (38) Vu, Q. A.; Fan, S.; Lee, S. H.; Joo, M.-K.; Yu, W. J.; Lee, Y. H. Near-Zero Hysteresis and Near-Ideal Subthreshold Swing in h-BN Encapsulated Single-Layer MoS<sub>2</sub> Field-Effect Transistors. *2D Mater.* **2018**, *5*, No. 031001.
- (39) Lin, Y.-C.; Lu, C.-C.; Yeh, C.-H.; Jin, C.; Suenaga, K.; Chiu, P.-W. Graphene Annealing: How Clean Can It Be? *Nano Lett.* **2012**, *12*, 414–419.
- (40) Rosenberger, M. R.; Chuang, H. J.; McCreary, K. M.; Hanbicki, A. T.; Sivaram, S. V.; Jonker, B. T. Nano-“Squeegee” for the Creation of Clean 2D Material Interfaces. *ACS Appl. Mater. Interfaces* **2018**, *10*, 10379–10387.
- (41) Rosenberger, M. R.; Chuang, H. J.; Phillips, M.; Oleshko, V. P.; McCreary, K. M.; Sivaram, S. V.; Hellberg, C. S.; Jonker, B. T. Twist Angle-Dependent Atomic Reconstruction and Moiré Patterns in Transition Metal Dichalcogenide Heterostructures. *ACS Nano* **2020**, *14*, 4550–4558.
- (42) Goossens, A. M.; Calado, V. E.; Barreiro, A.; Watanabe, K.; Taniguchi, T.; Vandersypen, L. M. K. Mechanical Cleaning of Graphene. *Appl. Phys. Lett.* **2012**, *100*, No. 073110.
- (43) Lembke, D.; Bertolazzi, S.; Kis, A. Single-Layer MoS<sub>2</sub> Electronics. *Acc. Chem. Res.* **2015**, *48*, 100–110.
- (44) Manzeli, S.; Ovchinnikov, D.; Pasquier, D.; Yazyev, O. V.; Kis, A. 2D Transition Metal Dichalcogenides. *Nat. Rev. Mater.* **2017**, *2*, 17033.
- (45) Chhowalla, M.; Jena, D.; Zhang, H. Two-Dimensional Semiconductors for Transistors. *Nat. Rev. Mater.* **2016**, *1*, 16052.
- (46) Rai, A.; Movva, H.; Roy, A.; Taneja, D.; Chowdhury, S.; Banerjee, S. Progress in Contact, Doping and Mobility Engineering of MoS<sub>2</sub>: An Atomically Thin 2D Semiconductor. *Crystals* **2018**, *8*, 316.
- (47) Lee, C.; Rath, S.; Khan, M. A.; Lim, D.; Kim, Y.; Yun, S. J.; Youn, D.-H.; Watanabe, K.; Taniguchi, T.; Kim, G.-H. Comparison of Trapped Charges and Hysteresis Behavior in HBN Encapsulated Single MoS<sub>2</sub> Flake Based Field Effect Transistors on SiO<sub>2</sub> and HBN Substrates. *Nanotechnology* **2018**, *29*, 335202.
- (48) Son, J.; Kwon, J.; Kim, S.; Lv, Y.; Yu, J.; Lee, J.-Y.; Ryu, H.; Watanabe, K.; Taniguchi, T.; Garrido-Menacho, R.; et al. Atomically Precise Graphene Etch Stops for Three Dimensional Integrated Systems from Two Dimensional Material Heterostructures. *Nat. Commun.* **2018**, *9*, 3988–3989.
- (49) Wang, J.; Yao, Q.; Huang, C.-W.; Zou, X.; Liao, L.; Chen, S.; Fan, Z.; Zhang, K.; Wu, W.; Xiao, X.; et al. High Mobility MoS<sub>2</sub> Transistor with Low Schottky Barrier Contact by Using Atomic Thick h-BN as a Tunneling Layer. *Adv. Mater.* **2016**, *28*, 8302–8308.
- (50) Cui, X.; Shih, E.-M.; Jauregui, L. A.; Chae, S. H.; Kim, Y. D.; Li, B.; Seo, D.; Pistunova, K.; Yin, J.; Park, J.-H.; et al. Low-Temperature Ohmic Contact to Monolayer MoS<sub>2</sub> by van Der Waals Bonded Co/h-BN Electrodes. *Nano Lett.* **2017**, *17*, 4781–4786.
- (51) Song, B.; Xi, N.; Yang, R.; Lai, K. W. C.; Qu, C. Video Rate Atomic Force Microscopy (AFM) Imaging Using Compressive Sensing. In *2011 11th IEEE International Conference on Nanotechnology*; IEEE: 2011; pp. 1056–1059.
- (52) Mak, K. F.; Lee, C.; Hone, J.; Shan, J.; Heinz, T. F. Atomically Thin MoS<sub>2</sub>: A New Direct-Gap Semiconductor. *Phys. Rev. Lett.* **2010**, *105*, 136805.
- (53) Splendiani, A.; Sun, L.; Zhang, Y.; Li, T.; Kim, J.; Chim, C. Y.; Galli, G.; Wang, F. Emerging Photoluminescence in Monolayer MoS<sub>2</sub>. *Nano Lett.* **2010**, *10*, 1271–1275.
- (54) Moody, G.; Kavir Dass, C.; Hao, K.; Chen, C. H.; Li, L. J.; Singh, A.; Tran, K.; Clark, G.; Xu, X.; Berghäuser, G.; et al. Intrinsic Homogeneous Linewidth and Broadening Mechanisms of Excitons in Monolayer Transition Metal Dichalcogenides. *Nat. Commun.* **2015**, *6*, 1–6.
- (55) Ajayi, O. A.; Ardelean, J. V.; Shepard, G. D.; Wang, J.; Antony, A.; Taniguchi, T.; Watanabe, K.; Heinz, T. F.; Strauf, S.; Zhu, X.-Y.; et al. Approaching the Intrinsic Photoluminescence Linewidth in Transition Metal Dichalcogenide Monolayers. *2D Mater.* **2017**, *4*, No. 031011.
- (56) Mouri, S.; Miyauchi, Y.; Matsuda, K. Tunable Photoluminescence of Monolayer MoS<sub>2</sub> via Chemical Doping. *Nano Lett.* **2013**, *13*, 5944–5948.
- (57) Conley, H. J.; Wang, B.; Ziegler, J. I.; Haglund, R. F., Jr.; Pantelides, S. T.; Bolotin, K. I. Bandgap Engineering of Strained Monolayer and Bilayer MoS<sub>2</sub>. *Nano Lett.* **2013**, *13*, 3626–3630.
- (58) Cadiz, F.; Courtade, E.; Robert, C.; Wang, G.; Shen, Y.; Cai, H.; Taniguchi, T.; Watanabe, K.; Carrere, H.; Lagarde, D.; et al. Excitonic Linewidth Approaching the Homogeneous Limit in MoS<sub>2</sub>-Based van Der Waals Heterostructures. *Phys. Rev. X* **2017**, *7*, No. 021026.
- (59) Mak, K. F.; He, K.; Lee, C.; Lee, G. H.; Hone, J.; Heinz, T. F.; Shan, J. Tightly Bound Trions in Monolayer MoS<sub>2</sub>. *Nat. Mater.* **2013**, *12*, 207–211.
- (60) Zhu, C. R.; Wang, G.; Liu, B. L.; Marie, X.; Qiao, X. F.; Zhang, X.; Wu, X. X.; Fan, H.; Tan, P. H.; Amand, T.; et al. Strain Tuning of Optical Emission Energy and Polarization in Monolayer and Bilayer MoS<sub>2</sub>. *Phys. Rev. B - Condens. Matter Mater. Phys.* **2013**, *88*, 121301.
- (61) He, K.; Poole, C.; Mak, K. F.; Shan, J. Experimental Demonstration of Continuous Electronic Structure Tuning via Strain in Atomically Thin MoS<sub>2</sub>. *Nano Lett.* **2013**, *13*, 2931–2936.
- (62) Laturia, A.; Van de Put, M. L.; Vandenberghe, W. G. Dielectric Properties of Hexagonal Boron Nitride and Transition Metal Dichalcogenides: From Monolayer to Bulk. *npj 2D Mater. Appl.* **2018**, *2*, 1–7.
- (63) Liang, J.; Xu, K.; Toncini, B.; Bersch, B.; Jariwala, B.; Lin, Y. C.; Robinson, J.; Fullerton-Shirey, S. K. Impact of Post-Lithography Polymer Residue on the Electrical Characteristics of MoS<sub>2</sub> and WSe<sub>2</sub> Field Effect Transistors. *Adv. Mater. Interfaces* **2019**, *6*, 1801321.
- (64) Late, D. J.; Liu, B.; Matte, H. S. S. R.; Dravid, V. P.; Rao, C. N. R. Hysteresis in Single-Layer MoS<sub>2</sub> Field Effect Transistors. *ACS Nano* **2012**, *6*, 5635–5641.
- (65) Ahn, J.-H.; Parkin, W. M.; Naylor, C. H.; Johnson, A. T. C.; Drndić, M. Ambient Effects on Electrical Characteristics of CVD-Grown Monolayer MoS<sub>2</sub> Field-Effect Transistors. *Sci. Rep.* **2017**, *7*, 4075.
- (66) Lee, S. Y.; Kim, U. J.; Chung, J.; Nam, H.; Jeong, H. Y.; Han, G. H.; Kim, H.; Oh, H. M.; Lee, H.; Kim, H.; et al. Large Work Function Modulation of Monolayer MoS<sub>2</sub> by Ambient Gases. *ACS Nano* **2016**, *10*, 6100–6107.
- (67) Liu, S.; Yuan, K.; Xu, X.; Yin, R.; Lin, D.-Y.; Li, Y.; Watanabe, K.; Taniguchi, T.; Meng, Y.; Dai, L.; et al. Hysteresis-Free Hexagonal Boron Nitride Encapsulated 2D Semiconductor Transistors, NMOS and CMOS Inverters. *Adv. Electron. Mater.* **2019**, *5*, 1800419.
- (68) Zheng, X.; Calò, A.; Albiseti, E.; Liu, X.; Alharbi, A. S. M.; Arefe, G.; Liu, X.; Spieser, M.; Yoo, W. J.; Taniguchi, T.; et al. Patterning Metal Contacts on Monolayer MoS<sub>2</sub> with Vanishing Schottky Barriers Using Thermal Nanolithography. *Nat. Electron.* **2019**, *2*, 17–25.
- (69) Liu, Y.; Wu, H.; Cheng, H. C.; Yang, S.; Zhu, E.; He, Q.; Ding, M.; Li, D.; Guo, J.; Weiss, N. O.; et al. Toward Barrier Free Contact to Molybdenum Disulfide Using Graphene Electrodes. *Nano Lett.* **2015**, *15*, 3030–3034.
- (70) Wang, Y.; Kim, J. C.; Wu, R. J.; Martinez, J.; Song, X.; Yang, J.; Zhao, F.; Mkhoyan, A.; Jeong, H. Y.; Chhowalla, M. Van Der Waals Contacts between Three-Dimensional Metals and Two-Dimensional Semiconductors. *Nature* **2019**, *568*, 70–74.
- (71) Kang, K.; Xie, S.; Huang, L.; Han, Y.; Huang, P. Y.; Mak, K. F.; Kim, C. J.; Muller, D.; Park, J. High-Mobility Three-Atom-Thick Semiconducting Films with Wafer-Scale Homogeneity. *Nature* **2015**, *520*, 656–660.
- (72) Smithe, K. K. H.; Suryavanshi, S. V.; Muñoz Rojo, M.; Tedjarati, A. D.; Pop, E. Low Variability in Synthetic Monolayer MoS<sub>2</sub> Devices. *ACS Nano* **2017**, *11*, 8456–8463.

(73) Chee, S.-S.; Seo, D.; Kim, H.; Jang, H.; Lee, S.; Moon, S. P.; Lee, K. H.; Kim, S. W.; Choi, H.; Ham, M.-H. Lowering the Schottky Barrier Height by Graphene/Ag Electrodes for High-Mobility MoS<sub>2</sub> Field-Effect Transistors. *Adv. Mater.* **2019**, *31*, 1804422.

(74) Yu, Z.; Ong, Z. Y.; Pan, Y.; Cui, Y.; Xin, R.; Shi, Y.; Wang, B.; Wu, Y.; Chen, T.; Zhang, Y. W.; et al. Realization of Room-Temperature Phonon-Limited Carrier Transport in Monolayer MoS<sub>2</sub> by Dielectric and Carrier Screening. *Adv. Mater.* **2016**, *28*, 547–552.

(75) Chang, H. Y.; Zhu, W.; Akinwande, D. On the Mobility and Contact Resistance Evaluation for Transistors Based on MoS<sub>2</sub> or Two-Dimensional Semiconducting Atomic Crystals. *Appl. Phys. Lett.* **2014**, *104*, 113504.

(76) Radisavljevic, B.; Kis, A. Mobility Engineering and a Metal–Insulator Transition in Monolayer MoS<sub>2</sub>. *Nat. Mater.* **2013**, *12*, 815–820.

(77) Li, L. H.; Santos, E. J. G.; Xing, T.; Cappelluti, E.; Roldán, R.; Chen, Y.; Watanabe, K.; Taniguchi, T. Dielectric Screening in Atomically Thin Boron Nitride Nanosheets. *Nano Lett.* **2014**, *15*, 218–223.

(78) Zou, X.; Huang, C.-W.; Wang, L.; Yin, L.-J.; Li, W.; Wang, J.; Wu, B.; Liu, Y.; Yao, Q.; Jiang, C.; et al. Dielectric Engineering of a Boron Nitride/Hafnium Oxide Heterostructure for High-Performance 2D Field Effect Transistors. *Adv. Mater.* **2016**, *28*, 2062–2069.

(79) Giannazzo, F.; Greco, G.; Roccaforte, F.; Sonde, S. Vertical Transistors Based on 2D Materials: Status and Prospects. *Crystals* **2018**, *8*, 70.

(80) Britnell, L.; Gorbachev, R. V.; Jalil, R.; Belle, B. D.; Schedin, F.; Mishchenko, A.; Georgiou, T.; Katsnelson, M. I.; Eaves, L.; Morozov, S. V.; et al. Field-Effect Tunneling Transistor Based on Vertical Graphene Heterostructures. *Science* **2012**, *335*, 947–950.

(81) Georgiou, T.; Jalil, R.; Belle, B. D.; Britnell, L.; Gorbachev, R. V.; Morozov, S. V.; Kim, Y. J.; Gholinia, A.; Haigh, S. J.; Makarovskiy, O.; et al. Vertical Field-Effect Transistor Based on Graphene-WS<sub>2</sub> Heterostructures for Flexible and Transparent Electronics. *Nat. Nanotechnol.* **2013**, *8*, 100–103.

(82) Wang, D.; Che, S.; Cao, G.; Lyu, R.; Watanabe, K.; Taniguchi, T.; Lau, C. N.; Bockrath, M. Quantum Hall Effect Measurement of Spin-Orbit Coupling Strengths in Ultraclean Bilayer Graphene/WSe<sub>2</sub> Heterostructures. *Nano Lett.* **2019**, *19*, 7028–7034.

(83) Wakafuji, Y.; Moriya, R.; Masubuchi, S.; Watanabe, K.; Taniguchi, T.; MacHida, T. 3D Manipulation of 2D Materials Using Microdome Polymer. *Nano Lett.* **2020**, *20*, 2486–2492.

(84) Garcia, R.; Knoll, A. W.; Riedo, E. Advanced Scanning Probe Lithography. *Nat. Nanotechnol.* **2014**, *9*, 577–587.

(85) Gorbachev, R. V.; Riaz, I.; Nair, R. R.; Jalil, R.; Britnell, L.; Belle, B. D.; Hill, E. W.; Novoselov, K. S.; Watanabe, K.; Taniguchi, T.; et al. Hunting for Monolayer Boron Nitride: Optical and Raman Signatures. *Small* **2011**, *7*, 465–468.